

DYNAMIC OVERTURNING CAPACITY OF ROCKING PRECAST THIN WALL STRUCTURES

Nor Hayati binti Abdul Hamid¹, J.B Mander² and Iwan Surdano³

¹Lecturer, Faculty of Civil Engineering, Universiti Teknologi MARA 40450 UiTM, Shah Alam, Selangor

²Professor, Department of Civil Engineering, University of Canterbury, New Zealand

³Project Engineer, Baker Consultant, Wellington, New Zealand

E-mail: abdulhamid_nrhyt@yahoo.com

ABSTRACT

Most of the damages in precast wall panels occur within the plastic hinge zone (PHZ) which located at one-third bottom height of the wall. Fixed-base monolithic walls panels are commonly used in the construction of low, medium and high-rise buildings where the connection between wall and foundation beam is vulnerable to damage during earthquake. Damage Avoidance Design (DAD) is proposed in this paper in order to reduce the damage significantly and remain functional after earthquake. To validate and prove the level of damage, a specimen is designed, constructed, tested and analysed in this research. A slender wall panel with size of 3000x800x50mm is tested on shaking table under a few earthquake input such as white noise excitation, impulse excitation and Taft ground motion scaled to 0.2g PGA. Data collection and some visual observation are made during testing where the wall experienced minor damage because the bottom part of wall is steel-armoured and the wall is rocking steel-on-steel bed. A pair of unbonded post-tensioned tendons was used to provide self-centring and avoid any residual displacement during rocking mechanism. The amount of energy dissipated is also calculated and compare between experimental and theoretical values so that some correlation can be determined. In this experiment, the rocking damping is 0.12% and upper bound of hysteretic damping is 5%. Thus, it is recommended to use 12% for effective damping in designing precast thin wall panel which proved to have minimal damage through experimental results obtained.

Keywords: Damage Avoidance Design and Thin Precast Wall Panel, Effective Damping, Hysteretic Damping, PGA (Peak Ground Acceleration), Radiation Damping

1.0 INTRODUCTION

In the construction of precast buildings, most of precast wall panels are attached to the foundation beam using fixed-based connection. Under moderate/severe earthquake events, the damage is expected to occur at fixed base connection due to plastic hinge zone (PHZ) mechanism at wall-foundation interfaces. Moreover, the collapse of a thin wall might occur due to instability and buckling problems. It is suggested that the fixed-base connection can be replaced by steel-armoured rocking base connection where its performance can be markedly improved and damage essentially eliminated [1]. Based on the experimental work [1], the results demonstrated that the viability of rocking connection by conducting a proof-of-concept experiment on a relatively thick wall (height to thickness ratio of 30:1) under quasi-static reversed cyclic loading. Therefore, this study continues with two main differences as compared with work done by Holden *et al.*[1]. Firstly, the slenderness ratio for thin wall was 60:1 which represented a modern warehouse structure. Secondly, this experimental work was conducted on a shaking table using a real ground motion (earthquake excitation) as input.

This study will also examine the dynamic overturning capacity of a rocking wall along with the components of damping associated with rocking. Capacity spectrum method will be adopted in prototype design and validated using experimental work. Final conclusions and recommendations are drawn based on the efficiency of thin walls with armoured rocking base connections for the construction of prototype commercial and industrial facilities.

2.0 FINDINGS FROM PREVIOUS RESEARCH

The study of seismic performance of rocking structures is not new and was started 40 years ago by Housner [2] who sought to explain why certain tall golf-ball-on-tee type water reservoirs did not collapse during the earthquake events. He examined the dynamic performance of unrestrained rocking rigid using rocking connections. Some of the examples using this concept are the South Rangitikei Railway Bridge with rocking piers that incorporates energy dissipation devices and a rocking chimney at the Christchurch Airport in New Zealand.

Priestley and Tao [3] conducted an analytical study on seismic response of precast prestressed concrete frames using partially unbonded tendons but they did not consider radiation damping in their analysis, presumably because the impacts were not directly onto the ground where energy can be dissipated. Later on, Priestley and MacRae [4] verified the analysis by conducting beam-to-column joint subassemblages using partially debonded prestressing tendons. The concept of unbonded tendon was further investigated by Priestley *et al.*[5] looking into the five-storey PRESS building which was designed, constructed and tested at the University of California, San Diego, U.S.A.

Mander and Cheng [6] developed a new design philosophy using rocking column piers known as Damage Avoidance Design (DAD) as further development in capacity design principle. This design philosophy is to mitigate the earthquake induced damage on structures which often prevents structures from performing their normal service after a major earthquake event. Another study

was carried out by Garcia [7] who had tested on a one-quarter scale bridge model with rocking piers. Good dynamic performance was observed during the testing with large seismic deformations being able to be accommodated without inducing any structural damage. To validate on DAD philosophy, Ajrab [8] tested the frame-wall structure prototypes together with special tendon-damper systems. Experimental results showed that the structure can sustain higher level of inter-storey displacement with minimal damage. Hamid *et al.*[9] proved that DAD philosophy is also applicable for the construction of rocking precast hollow core wall in single storey warehouse buildings. Experimental observations of single wall tested on shaking table and multi-panel walls tested on strong floor did not show any damage on the structures up to 3.0% drift.

Many research were conducted using unbonded tendons and precast wall panel system. Kurama *et al.* [10] used analytical models to predict the behaviour of six six-storey prototype walls with unbonded post-tensioned tendons. Their studies proved that the unbonded post-tensioned precast walls have the capabilities to soften and undergo large non-linear lateral drift with little damage due to gap openings along the horizontal joints. Note that although this connection detail may be regarded as a rocking connection, it is unarmoured and can not therefore perform in accordance with DAD principles. Rahman and Restrepo [11] also conducted rocking connection tests using three half-scale precast concrete wall models were built in the variation of gravity loads and the occurrence of energy dissipating devices. But they did not protect bottom of the wall. Holden *et al.* [1] preceded the work by studying two half-scale precast walls, one with monolithic emulation connection and the other wall with an armoured rocking connection. Thus, compare their seismic performance under reversed quasi-static loading. Continuation from Holden *et al.*[1] work, this study is seek to use DAD philosophy in designed, construction and testing of precast thin/slender wall panel under past earthquake excitation.

3.0 BASE SHEAR CAPACITY OF A ROCKING WALL

Figure 1 shows the rocking mechanism of thin wall with a pair of flexural energy dissipators. The wall base is armoured with the steel and seated on a steel plate that is secured within the foundation beam/footing. Under dynamic loading, the wall is expected to uplift and rock as shown in Figure 1(a). The resistance of wall can be uncoupled by energy dissipating damper force (P_D), gravity force (P_G) and unbonded prestressing strands force (P_p) as shown in Figure 1(b) and (c). By taking moments about rocking toe of the wall, the base shear capacity is given by

$$C_c = F = \frac{W}{H} = (P_D + P_G + P_p) \frac{B}{2H} \quad (1)$$

where F = lateral force induced at the top of the wall by total inertia load; H = height of the wall; P_D = vertical resistance from the dissipators; P_G = gravitational loads; P_p = prestressing forces and B = width of the wall. The vertical and horizontal equilibrium requires that

$$P = P_D + P_G + P_p; F = F_D + F_G + F_p \quad (2)$$

in which P = total vertical resistance capacity; F_D , F_G , F_p are the equivalent lateral forces that can be balanced by the vertical capacity from the dissipators, gravity and prestress, respectively.

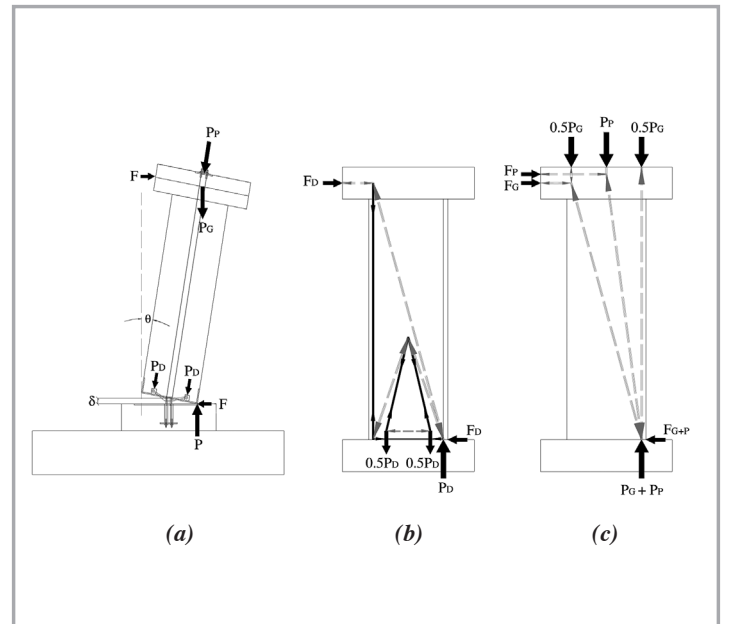


Figure 1: Rocking mechanism of thin wall; (a) vertical resistance components to the lateral load; (b) dissipator resistance; and (c) gravity and prestressing resistance

Forces P_p and P_D and hence F_p and F_D vary depending on the lateral drift followed by uplifting. This is based on rigid body kinematics as follows.

Consider a wall drift of θ . The prestressing tendons are elongated by:

$$\delta = \theta \frac{B}{2} \quad (3)$$

Forces in the tendons and dissipators will change significantly. Thus, the change of prestressing force is equal to

$$\Delta P_p = \delta \frac{A_p E_s}{L_t} = \frac{1}{2} \theta \frac{B A_p E_s}{L_t} \quad (4)$$

in which ΔP_p is the change in the prestress force (this should be added to the initial post-tensioning force, if any); A_p = area of prestressing strand; E_s = Young's modulus of the prestressing strand; and L_t = length of the tendon (this is slightly longer than H to include the effect of anchorage zone).

Figure 2 shows the overall effects of energy dissipator and unbonded prestressing in the thin wall. The overturning resistance of the dissipator contribution is added to the bilinear elastic response of the rocking post-tensioned wall, with its effect shown in the shaded zone in Figure 2(a). With lateral force increments the system moves from point 0 to point 1 where the system starts to rock. At point 2 the lateral displacement reaches the point where arms of the energy dissipators yield simultaneously. As the wall continues to drift a constant resistance of the yielding dissipators is provided as the system moves toward point 3. Upon reaching a peak displacement (drift) the velocity reverses and the system unloads. If the dissipators were truly elasto-plastic then the load path would be via point 4. However, in reality, due to the Bauschinger effect in steel unloading goes directly from 3 to 5. The energy enclosed within the loop shaded in Figure 2(b) provides hysteretic damping. However, this is most easily treated as equivalent viscous damping as discussed in the following section.

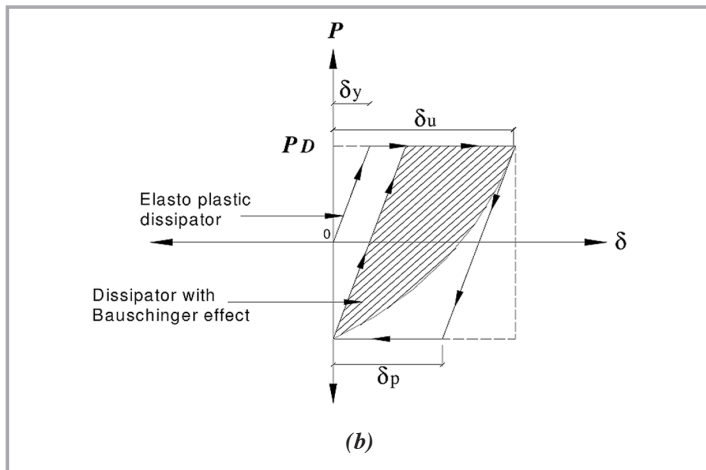
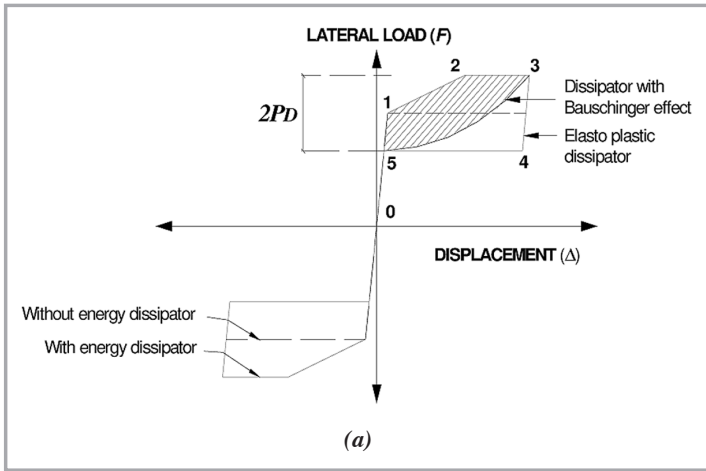


Figure 2: Rocking behaviour with supplemental steel energy dissipator; (a) flag-shape for a rocking wall and (b) dissipator hysteretic loop

damping approach can be used to represent these types of damping as follows.

$$\xi_{eg} = \frac{\delta E}{2\pi F_{max} \Delta_{max}} = \frac{\delta E}{C_c^{max} W_x \Delta_{max}} \quad (6)$$

where Δ_{max} and F_{max} are the maximum displacement and lateral force $F_{max} = C_c^{max} W_x$, respectively; W_x = inertia load; C_c^{max} = base shear capacity at the peak displacement; δE = energy released over a complete full cycle.

4.1 RADIATION DAMPING

Under radiation damping, Mander and Cheng [6] defined the amount of energy dissipated from one impact per-half cycle as:

$$\frac{1}{2} \delta E = (1-r) E_p = (1-r) W_y \frac{B}{2H} \Delta \quad (7)$$

in which $W_y = P_G$ = gravity load from roof ; r = difference between kinetic energy before and after impact; and E_p = the potential energy after the impact.

Figure 3 shows the physical properties of a rocking wall which supplemental non-gravitational inertia load attached. The dissipated energy can be written as

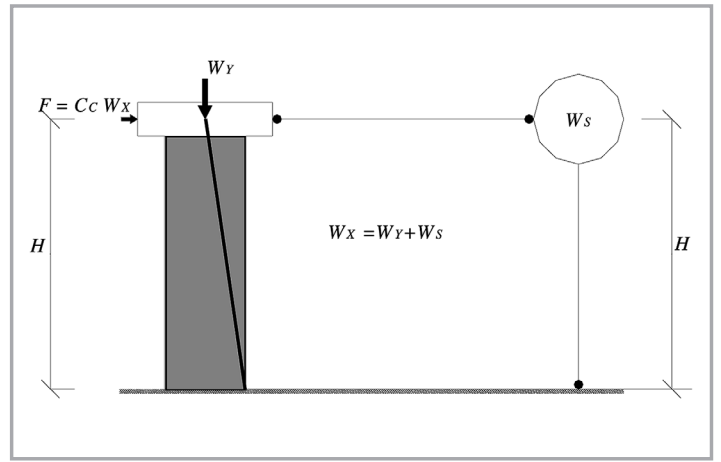


Figure 3: Rocking wall with supplemental non-gravitational inertia

$$r = \left[\frac{W_x R^2 - W_r \left(\frac{B}{2} \right)^2}{W_x R^2} \right]^2 = \left[1 - \frac{W_y \left(\frac{B}{2} \right)^2}{W_x R^2} \right]^2 \quad (8)$$

where R = the radius from the point of rotation to the inertial masses; $W_x = W_y + W_s$ is the combination of two inertia masses; W_s = non-gravitational inertia load; and W_y = vertical gravitational load. By expanding Equation (8) will give

$$r = \left[1 - \frac{W_y \left(\frac{B}{2} \right)^2}{W_y \left(\left(\frac{B}{2} \right)^2 + \left(\frac{H}{2} \right)^2 \right) + W_s \left(\left(\frac{B}{2} \right)^2 + H^2 \right)} \right]^2 \quad (9)$$

which can be simplified as

$$r = \left[1 - \frac{\left(\frac{B}{2H} \right)^2}{\frac{W_x}{W_y} \left(1 + \left(\frac{B}{2H} \right)^2 \right) - \frac{3}{4}} \right]^2 \quad (10)$$

The values of r are typically small; therefore the quantity $(1-r)$ in Equation (7) can be simplified using binomial expansion to give

$$1 - r \approx \frac{2 \left(\frac{W_y}{W_x} \right) \left(\frac{B}{2H} \right)^2}{\left(1 + \left(\frac{B}{2H} \right)^2 \right) - \frac{3}{4} \left(\frac{W_x}{W_y} \right)} \quad (11)$$

Rearranging the base shear capacity (CC):

$$C_c = \frac{F}{W_x} = \frac{P \left(\frac{B}{2} - \Delta \right) \frac{I}{H}}{W_x} = \frac{P_G + P_P}{W_x} \left(1 + \frac{P_D}{P_G + P_P} \right) \left(\frac{B}{2H} - \theta \right) \quad (12)$$

where θ = the system rotation (Δ/H). By substituting equation (7) and (12) into equation (6) gives:

$$\xi_{rocking} = \frac{(1-r)}{\pi} \frac{W_y B \Delta}{2H(W_x C_c) \Delta} \quad (13)$$

For small drift (θ), the radiation damping (for a complete cycle) can be written as

$$\xi_{rocking} = \frac{\frac{4}{\pi} \left(\frac{W_y}{W_x} \right) \left(\frac{B}{2H} \right)^2}{\left(1 + \left(\frac{B}{2H} \right)^2 - \frac{3}{4} \frac{W_y}{W_x} \right) \left(1 + \frac{P_D + P_P}{W_y} \right)} \quad (14)$$

This value of radiation damping is relatively independent to the uplift amplitude for the rocking system.

4.2 HYSTERETIC DAMPING

The energy in one half-cycle can be calculated using effective area within points 1 to 5 in Figure 2(a) as

$$\frac{1}{2} \delta E = \eta 2 P_D \left(\frac{B}{2H} \right) \Delta_{max} = \eta 2 P_D \quad (15)$$

in which η = efficiency factor relating the area of the enclosed half loop (rectangular) to the effective elasto-plastic area. Based on dissipator tests, $\eta = 0.33$ (for the first peak cycle) that accounts for the Bauschinger effect. In equation (15), P_D = dissipator capacity; and the terms within the first parenthesis represent the lateral capacity contribution to the overturning resistance arising from the dissipators alone. By substituting equation (15) to equation (7) gives:

$$\xi_{hysteretic} = \frac{0.1}{C_c^{max}} \frac{P_D}{W_x} \left(\frac{B}{H} \right) \left(1 - \frac{\Delta_{uplift}}{\Delta_{max}} \right) \quad (16)$$

The experimental work under medium displacement (1% drift) the wall specimen has an upper bound of $\xi_{hysteretic} = 5\%$.

5.0 DESIGN OF ROCKING WALL PROTOTYPE

The structure design capacity can be determined by calculating the demand induced to the structure using design response spectra. The demand is related to the structural period (T) of vibration which can be written in the well-known form as:

$$T = 2 \pi \sqrt{\frac{m}{K}} \quad (17)$$

where m = mass = W/g and K = stiffness. This can be expanded in terms of any nonlinear system where $K = F/\Delta$ and $C_c = F/W$ to give

$$T = 2 \pi \sqrt{\frac{W}{g} \frac{\Delta}{F}} = \sqrt{\frac{\Delta}{g C_c}} \quad (18)$$

where C_c = normalised base shear capacity at the maximum response; g = gravitational acceleration and Δ = maximum response displacement. For moderate to long periods, as shown in Figure 4(a), the spectral base shear demand (C_D) can be written for any level of damping as follows

$$C_D = S_a(\xi) = \frac{SA}{T B_L} \quad (19)$$

in which S = soil amplification factor, A = peak ground acceleration, T = period and B_L = factor accounting for a damping level above usual 5%. Pekcan *et al.* [12] have defined damping level as

$$B_L = \left(\frac{\xi_{eff}}{0.05} \right)^{0.3} \quad (20)$$

By setting base shear demand equal to the capacity ($C_D = C_c$) as shown in Figure 4(b), and substituting equation (18) into equation (19) gives the required seismic capacity in terms of the seismic demand as

$$C_c \Delta_{max} = \frac{g}{4\pi^2} \left(\frac{SA}{B_L} \right)^2 \quad (21)$$

The lateral strength can be obtained by

$$C_c = \frac{F}{W} = \frac{P}{W_x} \left(\frac{B}{2H} \right) \quad (22)$$

By expanding the term P , noting $\theta_{max} = \Delta_{max}/H$ and substituting equation (22) into equation (19) gives

$$\left(\frac{P_G + P_P + P_D}{W} \right) = \frac{g}{2\pi^2} \frac{I}{B\theta} \left(\frac{SA}{B_L} \right)^2 \quad (23)$$

The design example for rocking thin/slender wall panel is shown in Appendix A at the end of this paper.

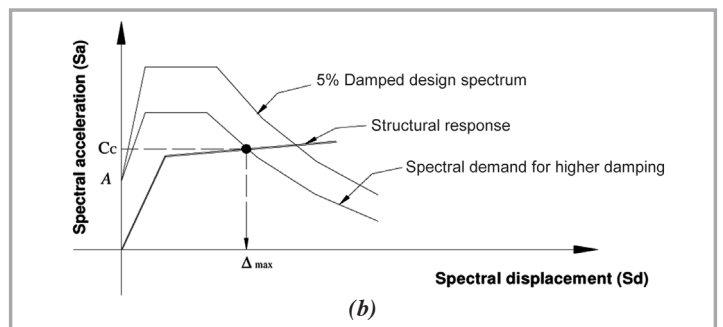
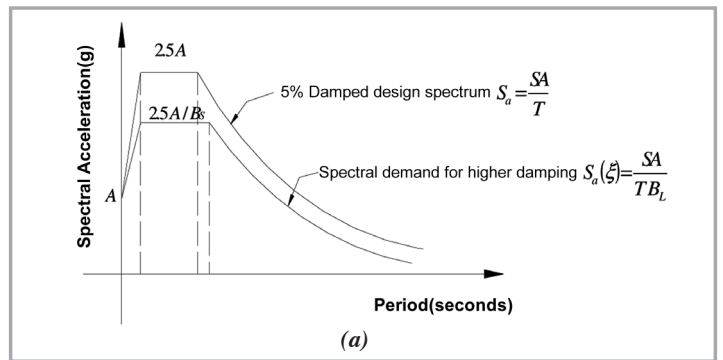


Figure 4: Spectral demand for systems with different viscous damping; (a) spectral acceleration demands for different level of viscous damping; (b) capacity spectrum method to predict the expected displacement of a system with higher level of viscous damping ($\xi_{eff} > 5\%$)

6.0 DESIGN AND DETAILING OF ROCKING WALL MODEL

The cantilever type energy dissipators were designed and installed at base-foundation wall model. A similar damping device was used and tested previously on the masonry rocking wall by Toranzo [13]. The dissipators were expected to yield in both tension and compression within a sufficient yielding length to prevent fatigue failures. Four energy dissipators each with a capacity of 7.5 kN, were used in addition to two-7mm diameter prestressing strands to provide a combined axial capacity of 117 kN at 3% drift. By converting the combined of P_p and P_p of 692kN on the prototype wall into the model, a minimum combined capacity of 97kN is required on 3/8 scaled model.

Figure 5 depicts the structural wall resisting lateral load induced by a combination of inertia load (W_s) and the gravitational load (W_g). The lateral resistances were provided by the gravity load (P_g), the prestressing force (P_p) and the energy dissipators (P_d). In predicting lateral load capacity by equalling the overturning moment caused by inertial load attached at the top of the wall to the resistance moment provided by the system. The $P-\Delta$ effect was taken into the consideration for the resistance calculation.

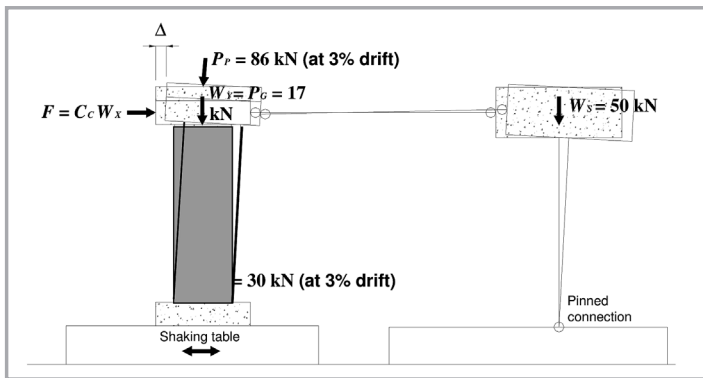


Figure 5: Lateral resisting components of the rocking wall

7.0 PHYSICAL MODELING AND EXPERIMENTAL WORK

Figure 6 presents the reinforcement detailing of thin wall specimen. The upper part of the wall carries a concrete block upon which another block was mounted as shown Figure 6(a). The percentage of longitudinal reinforcement was minimal (0.5%). Two longitudinal prestressing ducts were provided at the central region of the wall. The prestressing tendons were anchored into the foundation beam. The flexural mechanical energy dissipators were mounted at the base of the wall and anchored to steel block that tied back into the wall as shown Figure 6(b). Additional diagonal bars were also provided to help mitigate the high compression stresses near the rocking toe of the wall. A prestress force of 15 kN in each tendon was provided and anchored off at the top of the wall. Tensile test was carried out on the prestressing strand gave linear behaviour up to 1400 MPa with a Young's modulus of 190 GPa. The testing procedures of the model specimens were divided into three stages: (1) white-noise record excitations with low amplitudes to investigate the pre-rocking behaviour; (2) impulse tests to verify the experimental damping of the rocking system; and (3) earthquake excitation records to observe the rocking performance of the model under dynamic earthquake excitation. This specimen will be tested on shaking table subjected to white noise excitation, impulse test and scaled earthquake excitation. The results will be discussed in the following section.

8.0 EXPERIMENTAL RESULTS

8.1 WHITE NOISE EXCITATION

White noise acceleration records with peak ground acceleration of 0.02g and 0.05g were developed to investigate the pre-rocking behaviour of the wall panel. Whilst a pre-rocking behaviour was observed during 0.02g PGA white-noise excitation, a rocking behaviour occurred during the 0.05g PGA excitation. The results are presented in Figure 7. The white noise input is shown in Figure 7(a), and to this motion a maximum elastic relative displacement of 1.53 mm (0.05% drift) was observed [Figure 7(b)]. A natural period of 0.27 seconds and damping level of 0.36% [Figure 7(c)] were observed prior to rocking. The response acceleration-displacement diagram in Figure 7(d) resembles a straight line which can be taken as the stiffness of the system prior rocking. This value is agreed well with a theoretical prediction based on an uncracked section stiffness. A rocking mechanism was observed during the 0.05g PGA white-noise excitation with 5.73 mm maximum relative displacement was recorded during excitation, with an effective viscous damping factor from the frequency domain of 0.26%.

8.2 RESPONSE OF THIN WALL UNDER IMPULSE TEST

For the impulse tests, to avoid any stick-slip motion during experimental work, the shaking table was moved with a low velocity for 5 seconds and then half-sine pulse was applied as shown in Figures 8(a) and (b). Three impulse tests were conducted at 0.05g, 0.10g and 0.15g PGA (Peak Ground Acceleration). The sample result for 0.15g

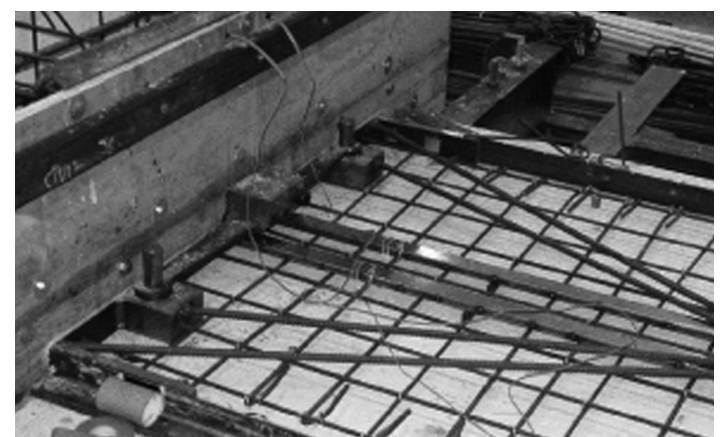
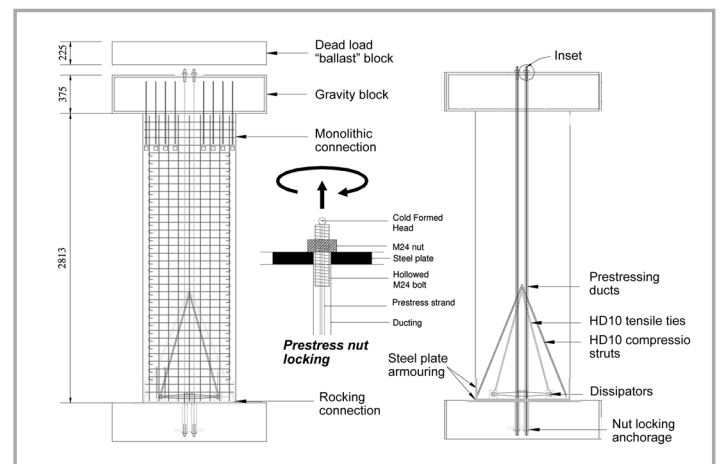


Figure 6: The rocking wall construction detail; (a) reinforcement layout of the specimen; (b) close up showing of triangular tension-compression struts

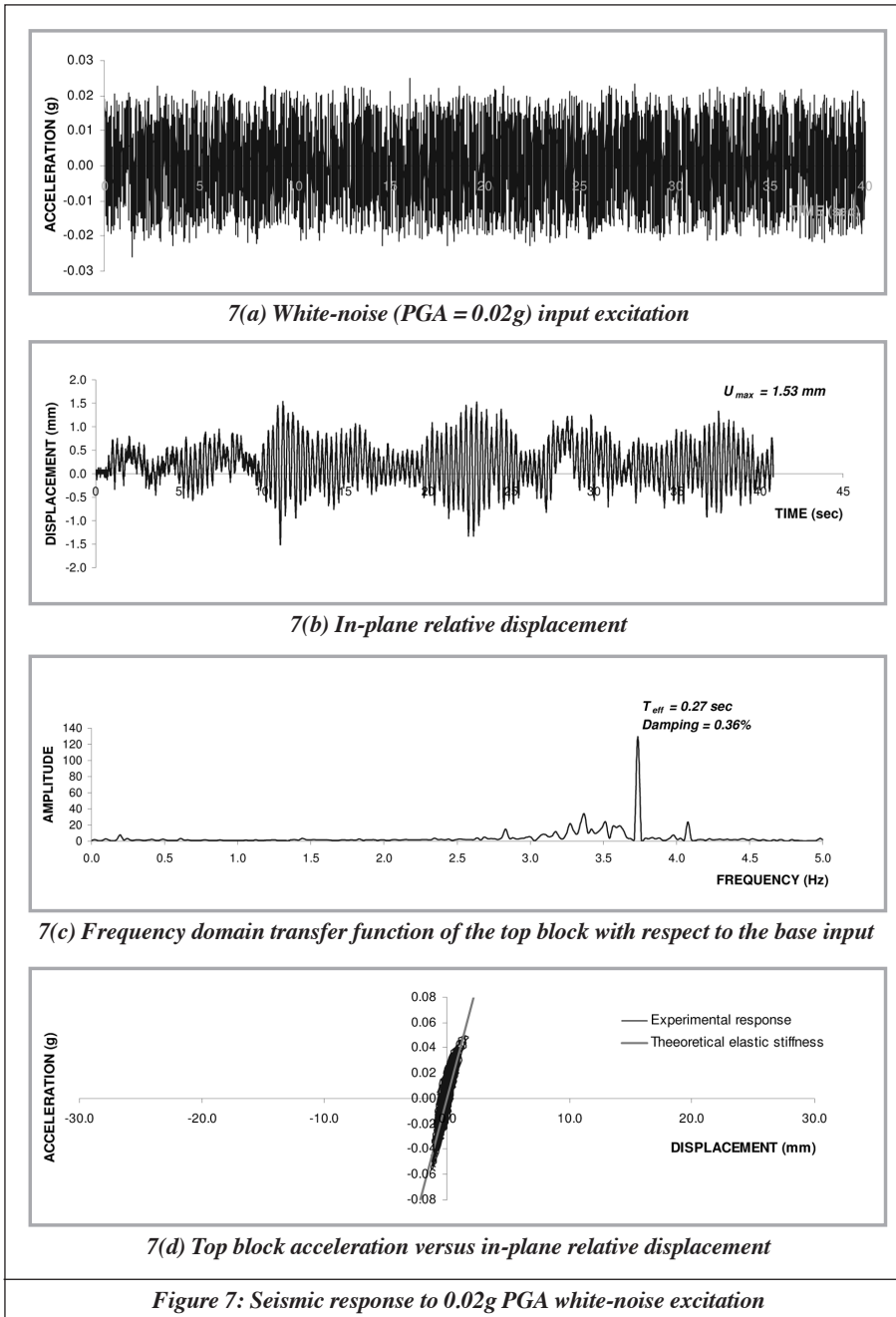


Figure 7: Seismic response to 0.02g PGA white-noise excitation

PGA on relative displacement is shown in Figure 8(c). As expected a logarithmic decay response was observed when rocking under free vibration. A maximum relative displacement of 25 mm (0.83% drift) was recorded during the 0.15g PGA impulse test with ± 2 mm lateral displacement was taken as the pre-rocking displacement. Figure 8(d) presents the viscous damping level of the experimental data from all three impulse tests. Table 1 summaries the experimental results from the impulse tests. While the pre-rocking periods of the structure from three different tests were relatively constant at around 0.26 seconds, the rocking period increased substantially as the drift of the structure increased.

Total effective viscous damping (ξ_{eff}) can be calculated from the experimental data given the record peak displacement. Given the peak displacement from experimental cycles:

$$\xi_{eff} = \frac{1}{2\pi j} \ln \frac{u_i}{u_{i+j}} \quad (24)$$

where u_i = peak displacement where the first cycles is measured; u_{i+j} = peak displacement after j cycles. Between consecutive cycles the effective damping reduces to:

$$\xi_{eff} = -15.92 \ln \left(\frac{u_{i+1}}{u_i} \right) \% \quad (25)$$

It is evident that the damping level was higher when the lateral displacement was relatively small. Ranging between 0.2 and 0.5% drift the damping level is relatively constant at about 3%. The effective viscous damping then started to peak up at larger lateral displacements due to the activation of the hysteretic damping from the steel energy dissipators. From the uplift test result, it was appeared that for the same cycle amplitude the dissipated energy during first peak cycle is larger than the following cycles. This ratio is significantly larger for small amplitudes. Marginally larger radiation damping was calculated for small amplitudes due to smaller energy from the overall system. At maximum in-plane drift of 0.6%, total damping of 7% was observed for one peak cycle. Intrinsic damping can only be inferred from the test results as $\xi_{intrinsic} = \xi_{eff} - \xi_{rocking} - \xi_{hysteretic}$. From the results presented in Figure 8, this appears to be $\xi_{intrinsic} = 3\%$.

8.3 RESPONSE OF THIN WALL UNDER EARTHQUAKE MOTION

The Taft ground motion scaled to a PGA of 0.2g is presented in Figure 9(a) while Figure 9(b) shows the in-plane relative displacement to this ground motion in the time domain. A maximum lateral displacement of 31 mm (1.04% drift) was observed. Figure 9(c) shows the base shear-displacement diagram which compares theoretical prediction to the experimental response under cyclic loading. The strength capacity agrees well with the observed result, although for reasons to do with the aforementioned Bauschinger effect the effectiveness of the dissipators is reduced on cyclic loading. By plotting the base-shear capacity against the linear spectral demand as shown in Figure 9(d), it is possible to infer an expected response. As noted earlier the effective damping may be expected to lie between 4% and 7% implying expected response between 23 and 36 mm. This compares favourably with the observed maximum response of 32 mm. Note that Figure 9(d) is an “exact” form of the capacity spectrum method of analysis.

9.0 CONCLUSIONS

Based on this study, the following conclusions are drawn:

1. Satisfactory seismic performance under a moderate level of earthquake excitation was observed without any discernible damage. Moreover after each earthquake test the specimen returned to its original up-right position with no sign of residual deformation both in or out-of-plane.

Table 1: Impulse test

	Unit	IMP051	IMP101	IMP151
j		8	8	8
u_i		5	12	17
u_{i+j}		0.7	2.5	3
T_i		6.4	6.4	6.4
T_{i+j}		8.65	9.72	12.4
Drift		-0.23%	-0.49%	-0.76%
Rocking Period	sec	0.32	0.47	0.86
Rocking frequency	Hz	3.11	2.11	1.17
Damping		3.91%	3.12%	3.45%
b		6	6	6
T_a	sec	12.04	12.2	13.76
T_{a+b}	sec	13.62	13.78	15.5
Pre-rocking period	sec	0.26	0.26	0.29
Pre-rocking frequency	(Hz)	3.80	3.80	3.45

- The dynamic performance of the slender concrete wall with a rocking connection was significantly better when compared to the specimens with fixed base monolithic emulation. The application of the emerging Damage Avoidance design (DAD) philosophy appears to work well for thin walls.
- The provision of the flexural beam steel energy dissipators was a mixed success. Although these dampers give a marginal improvement by providing some additional overturning resistance, their hysteretic damping capabilities reduce the peak amplitude during rocking.
- Radiation damping can be very effective in mitigating rocking response. However for relatively slender bodies, and especially those with supplementary inertia weight (such as may be present in a real structural system), the effectiveness of radiation damping is markedly reduced. Other means of damping may be necessary to reduce the response of structures.

10.0 ACKNOWLEDGEMENTS

The authors wish to acknowledge the research funding from Building Research Association of New Zealand (BRANZ), Foundation Research Science and Technology of New Zealand (FRST) and Firth Industries for providing wet concrete and grouting cement.

APPENDIX A: DESIGN EXAMPLE

A typical single storey warehouse building is designed and to be constructed in the highest seismic hazard region such as Bandar Aceh, Sumatra. The Basic Design Earthquake (DBE) is 0.4g and Maximum Considered Earthquake (MCE) is 0.8g. The size of the warehouse is 60m long and 40m wide with spacing between rafters is 6m. The wall is 8m height, 1.2m width and 0.2m thick. The warehouse building is situated on intermediate soil, type b according to soil classification. The following assumptions are made for design purposes:

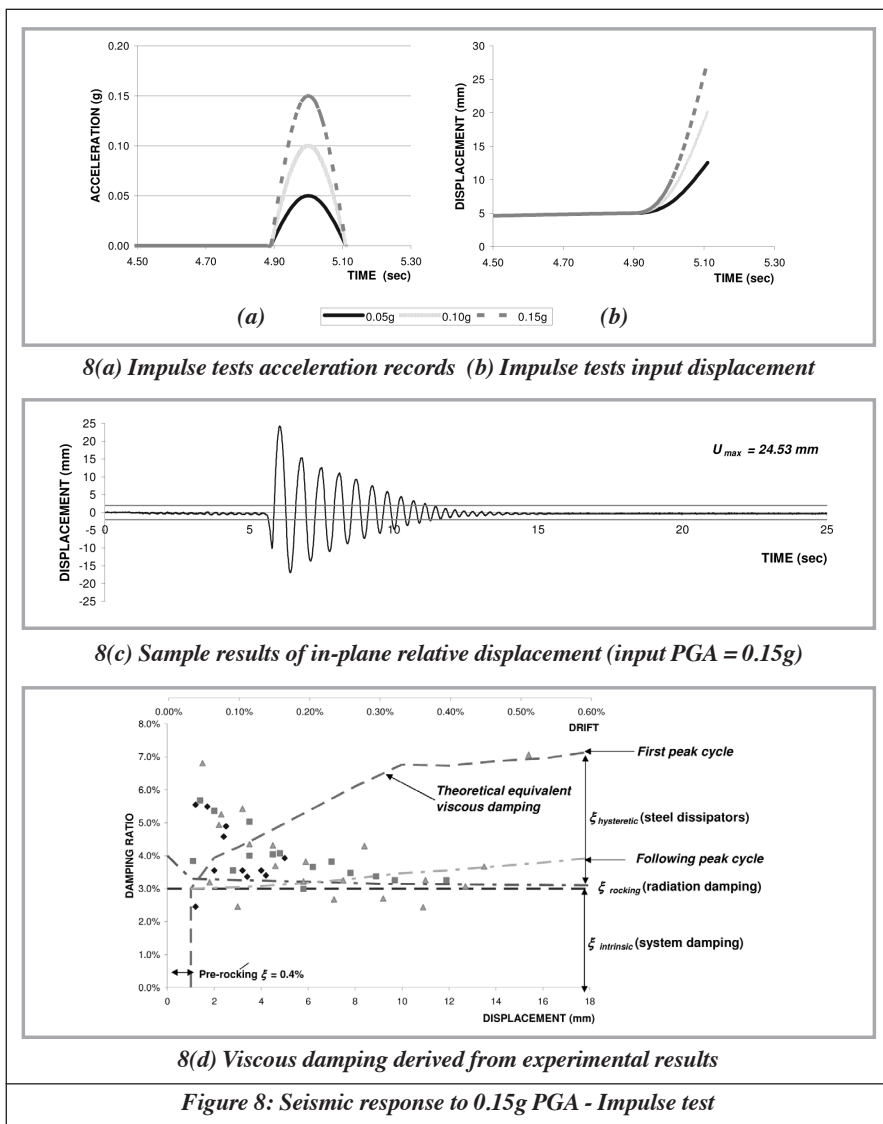
- Self-weight of the roof, $P_G = 17kN$
- Non-gravitational inertia load, $W_s = 50kN$
- The soil type factor, $S = 1.0$
- Compressive strength of concrete, $f_c = 50MPa$
- Acceleration of gravity, $g = 9.81m/s^2$
- At 1% drift, the values of $P_D = 20kN$ and $P_p = 48kN$

SOLUTION

Total gravity load, $W_x = W_s + W_y = 17kN + 50kN = 67kN$

The difference between kinetic energy before and after the impact can be calculated using Equation 10.

$$r = \left[1 - \frac{\left(\frac{1.2}{2(8)} \right)^2}{\frac{67}{50} \left(1 + \left(\frac{1.2}{2(8)} \right)^2 \right) - \frac{3}{4}} \right]^2 = 0.981$$



The radiation damping at 1% drift (ξ_{rocking}) can be calculated using Equation 14 as given below

$$\xi_{\text{rocking}} = \frac{4 \left(\frac{17}{67} \right) \left(\frac{1.2}{2(8)} \right)^2}{1 + \left(\frac{1.2}{2(8)} \right)^2 - \frac{3}{4} \left(\frac{17}{67} \right) \left(1 + \frac{20 + 48}{17} \right)} = 0.2\%$$

Base shear capacity at 1% drift is determined using Equation 12 as follows

$$C_c = \frac{17kN + 48kN}{67kN} \left(1 + \frac{20kN}{17kN + 48kN} \right) \left(\frac{1.2}{2(8)} - 0.01 \right) = 0.082$$

The hysteretic damping at 1% drift can be calculated using Equation 16

$$\xi_{\text{hysteretic}} = \frac{0.1}{0.082} \frac{20kN}{67kN} \left(\frac{1.2}{8} \right) \left(1 - \frac{80}{240} \right) = 3.64\%$$

Therefore, the total effective viscous damping as given in Equation 5 is $\xi_{\text{eff}} = 3\% + 3.64\% + 0.2\% = 6.84\%$

The reduction factor is calculated using equation 20 where

$$B_L = \left(\frac{0.684}{0.05} \right)^{0.3} = 2.19$$

Thus, the seismic capacity for this wall can be determine using equation 21 as

$$C_c = \frac{g}{\Delta_{\text{max}} 4\pi^2} \left(\frac{SA}{B_L} \right)^2 = \frac{9.81}{0.008 \times 4 \times \pi^2} \left(\frac{1.0}{2.19} \right)^2 = 0.647$$

The seismic capacity is mapped into the seismic demand of spectra design to determine the required amount of forces in resisting lateral forces (earthquake loading). The combination of forces in prestressing tendons and energy dissipators is used to design design energy dissipators and amount of steel required. ■

REFERENCES

- [1] Holden, T. J., Restrepo, J. I., Mander and J. B. *A Comparison of Seismic Performance of Precast Concrete Wall Construction: Emulation and Hybrid Approaches*, Research Report 2001-4, Department of Civil Engineering, University of Canterbury, Christchurch, New Zealand, 2003
- [2] Housner, G.W. *The Behaviour of Inverted Pendulum Structures during Earthquake*, Bulletin of Seismological Society of America, Vol. 53, No. 3, pp. 403-417, 1963.
- [3] Priestley, M. J. N., and Tao, J-T. *Seismic Response of Precast Prestressed Concrete Frames with Partially Debonded Tendons*, PCI Journal, Vol. 38, No. 1, January-February 1993, pp 58-69, 1993.
- [4] Priestley, M. J. N., and MacRae, G. A. *Seismic Testing of Precast Beam-to-Column Joint Assemblage with Unbonded Tendons*, PCI Journal, Vol. 41, No. 1, pp. 64-80, 1996.
- [5] Priestley, M. J. N., Sritharan, S., Conley, J. R. and Pampanin, S. *Preliminary Results and Conclusions from the PRESSS Five-Story Precast Concrete Test Building*, PCI Journal, Vol. 44, No. 6, pp 42-67, 1999.
- [6] Mander, J. B., and Cheng, C-T. *Seismic Resistance of Bridge Piers Based on Damaged Avoidance Design*, Technical Report NCEER-97-0014, NCEER, Department of Civil and Environmental Engineering, State University of New York at Buffalo, 1997.
- [7] Garcia, R. (1998). *Shaking Table Study of Rocking Column Bridge Based on Damage Avoidance Design*, Master Thesis, State University of New York at Buffalo, 1998.
- [8] Ajrab, J. J. *Rocking Wall-Frame Structures with Supplemental Damping Devices*, M.S. Thesis, State University of New York at Buffalo, 2000.
- [9] Hamid, N.H. and Mander, J.B. *Experimental study on bilateral seismic performance of precast hollow core wall using shaking table*, Proceeding of the tenth Asia-Pacific Conference on Structural and Construction (EASEC-10), Bangkok, Thailand, 3-5 August 2006.
- [10] Kurama, Y., Sause, R., Pessiki, S. and Lu, W-L. *Lateral Load Behavior and Seismic Design of Unbonded Post-Tensioned Precast Concrete Walls*, ACI Structural Journal, Vol. 96, No. 4, pp. 622-632, 1999.
- [11] Rahman, A. and Restrepo, J. I. *Earthquake Resistant Precast Concrete Buildings: Seismic Performance of Cantilever Walls Prestressed Using Unbonded Tendons*, Research Report, Department of Civil Engineering, University of Canterbury, 2000.
- [12] Pekcan, G., Mander, J. B. and Chen, S. S. *Fundamental Consideration for the Design of Non-Linear Viscous Damper*, Earthquake Engineering and Structural Dynamics, Vol. 28, pp 1405-1425, 1999.
- [13] Toranzo, L. A. *The Use of Rocking Walls in Confined Masonry Structures: a Performance-Based Approach*, PhD. Thesis, Department of Civil Engineering, University of Canterbury, 2002.

PROFILE



ENGR. DR NOR HAYATI BINTI ABDUL HAMID
 Engr. Dr Nor Hayati Abdul Hamid has been a lecturer at University Teknologi Mara, Shah Alam, Selangor for 15 years. She completed her PhD (Earthquake Engineering) from University of Canterbury, Christchurch, New Zealand in 2006. She received her Master of Science in Construction Management and Structural Engineering from University of Newcastle Upon Tyne, United Kingdom in 1993 and obtained her BSc (Civil Engineering) from University of Pittsburgh, United States of America in 1989. Her research interests are seismic performance of precast buildings under earthquake excitation, dynamic response of thin/slender wall, design of rocking precast hollow core walls under earthquake, cyclic behaviour of precast hollow core slabs and the interaction of beam-column joints under quasi-static reverse cyclic loading.